Journal of Organometallic Chemistry 895 (2019) 28–36

Contents lists available at ScienceDirect

Journal of Organometallic Chemistry

journal homepage: www.elsevier.com/locate/jorganchem

Photophysical properties and optical power limiting ability of Pt(II) polyynes bearing fluorene-type ligands with ethynyl units at different positions

Zhuanzhuan Tian, Xiaolong Yang, Boao Liu, Daokun Zhong, Guijiang Zhou*

MOE Key Laboratory for Nonequilibrium Synthesis and Modulation of Condensed Matter, State Key Laboratory for Mechanical Behavior of Materials, Department of Chemistry, School of Science, Xi'an Jiaotong University, Xi'an, 710049, PR China

ARTICLE INFO

Article history:
Received 14 April 2019
Received in revised form
15 May 2019
Accepted 21 May 2019
Available online 22 May 2019

Keywords:
Pt(II) polyynes
Triplet state
Transparency
Reverse saturable absorption
Optical power limiting

ABSTRACT

Two series of Pt(II) polyynes bearing fluorene-type ligands with ethynyl units at different positions have been synthesized. In the absorption spectra, the Pt(II) polyynes bearing fluorene-type ligands with ethynyl units at 3,6-position have blue-shift with respect to the corresponding analogs bearing fluorene-type ligands with ethynyl units at 2,7-position, showing better transparency in the visible light region. Moreover, the Pt(II) polyynes bearing fluorene-type ligands with ethynyl units at 3,6-position show stronger triplet emission than corresponding analogs bearing fluorene-type ligands with ethynyl units at 2,7-position in the photoluminescent (PL) spectra. Furthermore, these Pt(II) polyynes were applied to optical power limiting (OPL) field. The Pt(II) polyynes bearing fluorene-type ligands with ethynyl units at 2,7-position show better OPL performance than the corresponding analogs with fluorene-type ligands of ethynyl units at 3,6-position. Therefore, changing the position of the ethynyl units in fluorene-type ligands can not only effectively control the photophysical properties of the Pt(II) polyynes, but also has an important effect on their OPL ability.

1. Introduction

Recently, transition metal polyynes have attracted great attention due to their various applications, such as organic light-emitting diodes (OLEDs) [1,2], organic solar cells [3,4], ion sensors [5], nanomaterials [6,7] and so on. The extensive applications were based on their unique properties through the interaction of organic acetylide ligands and transition metal ions, such as Pt(II), Pd(II), Au(I), Hg(II) *etc*. Among them, Pt(II) polyynes are the most widely studied due to the advantages of stronger triplet emission, weak or no absorption in visible light region, solubility and so on [8,9]. Importantly, the properties of the Pt(II) polyynes, such as, triplet emission, absorption band, energy gap, can be fine-tuned by controlling chemical structures of the organic acetylide ligands [10,11]. This provides great convenience for furnish unique properties and applications to the Pt(II) polyynes.

So far, many organic acetylide ligands coordinating Pt(II) ions have been reported [8–19]. It is worth noting that fluorene acetylide ligands have attracted much attention due to their ease of chemical modification and tuning both electronic and geometric properties [20–23]. Moreover, the Pt(II) polyynes with fluorene-based ethynyl ligands can show high transparency in the visible-light region and good optical power limiting (OPL) ability. Based on their advantages, many reported fluorene acetylide ligands were designed by varying the substituents at their 9-position [22,24]. The photophysical properties and OPL ability of these Pt(II) polyynes can be effectively tuned by the designed ligands. Clearly, the ethynyl units at 2,7-position of the fluorene-type ligands were shifted to 3,6-positon, which can also provide an effective tuning the photophysical properties of the Pt(II) polyynes. However, the Pt(II) polyynes bearing the fluorene-type ligands with ethynyl units at 3,6-positon are relatively rare. Wong's group reported that the Pt(II) polyynes bearing 2, 8- diethynyl- 5, 5- dioxide-dibenzothiophene ligands show blue-shift effect in its absorption spectrum and stronger triplet emission with respect to the Pt(II) polyynes with 3, 7- diethynyl- 5, 5- dioxide-dibenzothiophene ligands [25]. The photophysical properties of the Pt(II) polyyne bearing 2, 8- diethynyl-dibenzothiophene ligands has also been reported by Wong's group [25], but its OPL behavior has not been studied yet. Hence, more analogs should be synthesized and

* Corresponding author.
E-mail address: zhougj@mail.xjtu.edu.cn (G. Zhou).

https://doi.org/10.1016/j.jorganchem.2019.05.022
0022-328X/

characterized to further explore their effect on the photophysical properties and OPL behavior of the Pt(II) polyynes.

On this basis, we designed two series of Pt(II) polyynes bearing fluorene-type ligands with ethynyl units at 2,7- and 3,6-position as well as different structures at 9-position. In the absorption spectra, the Pt(II) polyynes bearing fluorene-type ligands with ethynyl units at 3,6-positon can show blue-shift effect compared with the analogs bearing fluorene-type ligands with ethynyl units at 2,7-positon, indicating their better transparency in the visible-light region. Moreover, the Pt(II) polyynes bearing fluorene-type ligands with ethynyl units at 3,6-positon exhibit stronger triplet emission in their PL spectra. In addition, these Pt(II) polyynes can show obvious OPL response. Hence, the corresponding results will offer valuable information about controlling the photophysical properties and OPL performance of the Pt(II) polyynes by varying substitution position of the organic acetylide ligands.

2. Experimental

2.1. General information

Reagents were used as obtained from commercial suppliers except where indicated otherwise. All the solvents were purified by standard techniques. All reactions were preceded under a N_2 atmosphere. The reactions were monitored by thin-layer chromatography (TLC) with Merck pre-coated aluminum plates. Flash column chromatography and preparative TLC were carried out on silica gel. All Sonogashira reactions were carried out with standard Schlenk techniques.

2.2. Physical measurements

^1H, ^{13}C and ^{31}P NMR spectra were recorded using a Bruker AXS 400 MHz NMR spectrometer in $CDCl_3$ solvent. Fast atom bombardment (FAB) mass spectra were acquired using a Finnigan MAT SSQ710 system. The molecular weights were determined by Waters 2695 GPC and estimated by using a calibration curve of polystyrene standards in $CHCl_3$. UV–vis spectra were recorded on a PerkinElmer Lambda 950 spectrophotometer. The photoluminescent (PL) spectra were obtained with an Edinburgh Instruments FLS920 fluorescence spectrophotometer. The lifetime measurements at 298 K for the excited states were carried out using by a single photon counting spectrometer from Edinburgh Instruments FLS920 with a 360 nm ps LED lamp as the excitation source, while those at 77 K were recorded with the excitation from a Xenon flash lamp. Low-temperature PL spectra and lifetimes at 77 K were measured by dipping the degassed CH_2Cl_2 solution in a thin quartz tube into liquid nitrogen Dewar and recording data after standing 3 min. Fluorescent quantum yields (Φ_F) were determined in CH_2Cl_2 solution at 298 K, using the reference of quinine sulfate in 1.0 M H_2SO_4 (Φ_F *ca.* 0.56 at 334 nm and *ca.* 0.55 at 365 nm) [26].

2.3. Optical power limiting measurements

Optical power limiting (OPL) properties were recorded at 532 nm for Gaussian mode laser beam from a Q-switched Quantel Q-Smart 450 Nd:YAG laser with a repetition rate of 20 Hz. The laser beam was split into two beams by a beam splitter. One was used as the reference beam, which was directly received by a power detector (D1). The other was focused with a lens ($f = 20$ cm) for the sample measurement and then received by another power detector (D2) after transmitting through the sample. The sample to be measured was moved automatically along a rail to change the incident irradiance on it. The incident and transmitted powers were detected simultaneously by D1 and D2, individually. The OPL performance of each solution sample was measured in a 1 mm quartz cell filled with CH_2Cl_2 solution of the sample.

2.4. Computational details

Geometrical optimizations were performed using the popular B3LYP density functional theory (DFT). The 6-311G(d, p) basis set were used for C, H, O, S and P atoms, whereas effective core potentials with a LanL2DZ basis set were employed for Pt atom [27,28]. The energies of the excited states of the complexes were computed by TD-DFT based on all the ground-state geometries. All calculations were carried out by using the Gaussian 09 program [29].

2.5. Synthesis

The ethynyl aromatic ligands were prepared by the published Sonogashira coupling reaction [2,25,30]. All the synthetic procedures are described in the Electronic Supplementary Information (ESI).

2.6. General synthetic procedure for the Pt(II) polyynes

Under a N_2 atmosphere, the ethynyl aromatic ligand (1.0 equiv) and *trans*-[$PtCl_2(PBu_3)_2$] (1.0 equiv) were dissolved in Et_3N. Then, CuI (0.01 equiv) was added and the mixture reaction was stirred at room temperature for 12 h. After reaction, CuI was removed by centrifugation and the solvent was removed under reduced pressure. The obtained residue was dissolved in a small amount of CH_2Cl_2 and filtered by a syringe filter (PTFE, 0.45 mm) to remove the insoluble part. Then, it was precipitated in cold methanol and the collected precipitate was further purified by repeated precipitations to obtain the Pt(II) polyynes as a off-white solid in high yield.

C1-Pt: (Yield: 91%) ^1H NMR (400 MHz, $CDCl_3$): δ (ppm) 7.50 (d, 2H, Ar), 7.23–7.16 (m, 14H, Ar), 2.06 (br, 12H, PBu_3), 1.56–1.53 (m, 12H, PBu_3), 1.35–1.33 (m, 12H, PBu_3), 0.82 (t, 18H, PBu_3); ^{31}P NMR (161.9 MHz, $CDCl_3$): δ (ppm) 2.83; GPC: $M_n = 2.0 \times 10^4$ g mol^{-1}, PDI = 1.8 (against polystyrene standards).

O1-Pt: (Yield: 86%) ^1H NMR (400 MHz, $CDCl_3$): δ (ppm) 7.72–7.60 (m, 4H, Ar), 7.40 (d, 2H, Ar), 2.17 (br, 12H, PBu_3), 1.63 (br, 12H, PBu_3), 1.49–1.43 (m, 12H, PBu_3), 0.94 (t, 18H, PBu_3); ^{31}P NMR (161.9 MHz, $CDCl_3$): δ (ppm) 3.24; GPC: $M_n = 1.8 \times 10^4$ g mol^{-1}, PDI = 2.2 (against polystyrene standards).

S1-Pt: (Yield: 89%) ^1H NMR (400 MHz, $CDCl_3$): δ (ppm) 7.90 (d, 2H, Ar), 7.69 (s, 2H, Ar) 7.33 (d, 2H, Ar), 2.17 (br, 12H, PBu_3), 1.64 (m, 12H, PBu_3), 1.52–1.42 (m, 12H, PBu_3), 0.94 (t, 18H, PBu_3); ^{31}P NMR (161.9 MHz, $CDCl_3$): δ (ppm) 3.27; GPC: $M_n = 1.7 \times 10^4$ g mol^{-1}, PDI = 1.9 (against polystyrene standards).

PO1-Pt: (Yield: 85%) ^1H NMR (400 MHz, $CDCl_3$): δ (ppm) 7.65–7.46 (m, 7H, Ar), 7.37–7.35 (m, 4H, Ar), 2.05 (br, 12H, PBu_3), 1.57–1.53 (m, 12H, PBu_3), 1.38–1.32 (m, 12H, PBu_3), 0.83 (t, 18H, PBu_3); ^{31}P NMR (161.9 MHz, $CDCl_3$): δ (ppm) 33.67, 3.12; GPC: $M_n = 1.6 \times 10^4$ g mol^{-1}, PDI = 1.8 (against polystyrene standards).

C2-Pt: (Yield: 91%) ^1H NMR (400 MHz, $CDCl_3$): δ (ppm) 7.60–7.58 (m, 2H, Ar), 7.18 (m, 14H, Ar), 2.16 (br, 12H, PBu_3), 1.63 (br, 12H, PBu_3), 1.50–1.43 (m, 12H, PBu_3), 0.93 (t, 18H, PBu_3); ^{31}P NMR (161.9 MHz, $CDCl_3$): δ (ppm) 3.23; GPC: $M_n = 1.9 \times 10^4$ g mol^{-1}, PDI = 2.0 (against polystyrene standards).

O2-Pt: (Yield: 86%) ^1H NMR (400 MHz, $CDCl_3$): δ (ppm) 7.77 (s, 2H, Ar), 7.36 (s, 4H, Ar), 2.20 (br, 12H, PBu_3), 1.67 (m, 12H, PBu_3), 1.51–1.46 (m, 12H, PBu_3), 0.95 (t, 18H, PBu_3); ^{31}P NMR (161.9 MHz, $CDCl_3$): δ (ppm) 3.20; GPC: $M_n = 1.8 \times 10^4$ g mol^{-1}, PDI = 1.6 (against polystyrene standards).

S2-Pt: (Yield: 89%) ^1H NMR (400 MHz, $CDCl_3$): δ (ppm) 7.98 (s,

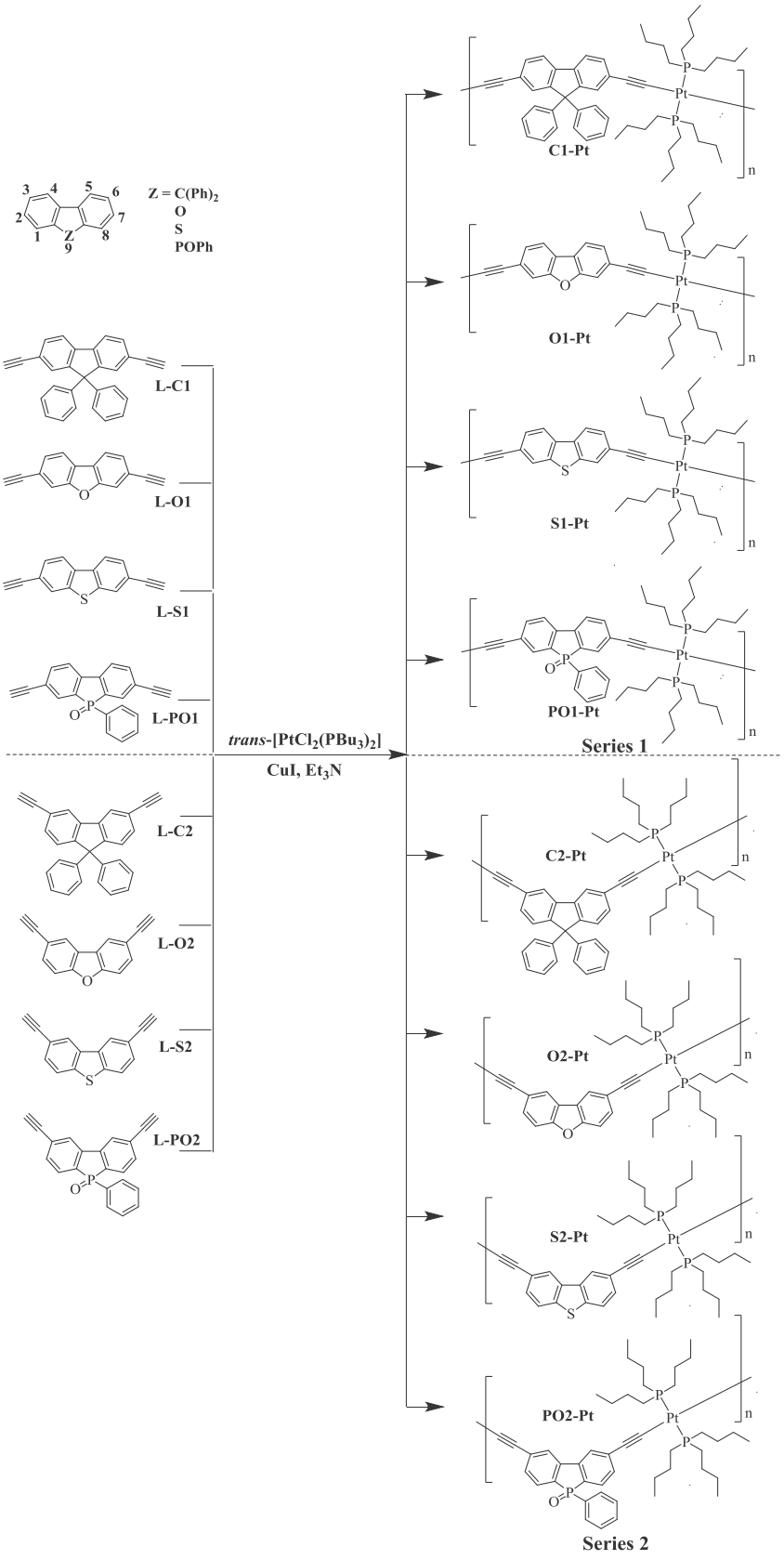

Scheme 1. Synthesis of the Pt(II) polyynes bearing fluorene-type ligands with ethynyl units at different positions.

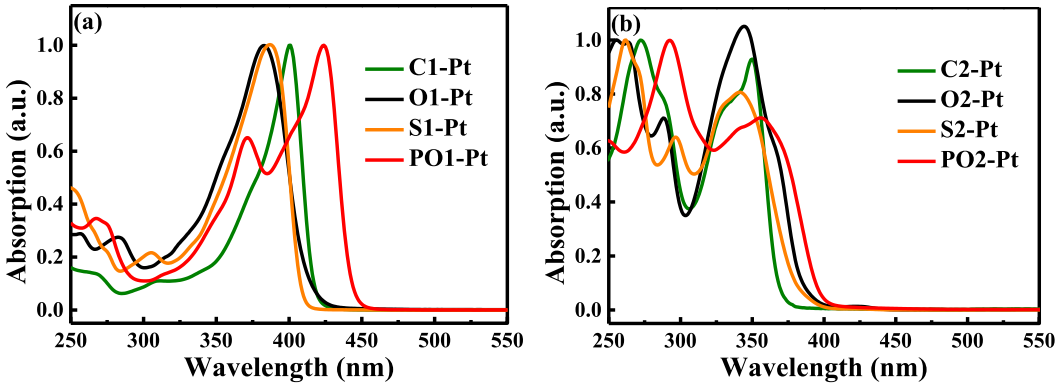

Fig. 1. UV–vis absorption spectra for the Pt(II) polyynes in CH_2Cl_2 at 298 K. (a) Series 1: **C1-Pt**, **O1-Pt**, **S1-Pt** and **PO1-Pt** (b) Series 2: **C2-Pt**, **O2-Pt**, **S2-Pt** and **PO2-Pt**.

Table 1
Photophysical data for the Pt(II) polyynes.

Compound	Absorption λ_{abs} (nm)[a] 298 K	Emission λ_{em} (nm)[a] 298 K/77 K	Φ_F[b] (%)	Lifetime of excited states[c] S_1 state (ns)/T_1 state (μs)	$\lambda_{cut\text{-}off}$ (nm)
C1-Pt	267, 310, 376^{sh}, 400	418,434,552,600/559,589,611	0.26	0.46 ns (418 nm)/103.6 μs (559 nm)	417
O1-Pt	250, 257, 283, 383	412, 438, 450^{sh}, 525/526, 550^{sh}, 567	1.08	0.54 ns (412 nm)/135 μs (526 nm)	411
S1-Pt	245, 265^{sh}, 274, 305, 387	406, 432, 530, 577/534, 567, 584	0.13	0.44 ns (406 nm)/89.3 μs (534 nm)	407
PO1-Pt	267, 315, 348^{sh}, 371, 406^{sh}, 423	446,463^{sh},586/602,656	0.69	0.55 ns (446 nm)/134.9 μs (602 nm)	443
C2-Pt	273, 288^{sh}, 329^{sh}, 350	366, 466, 509, 546/463, 497, 514, 538, 552	0.02	0.69 ns (366 nm)/64.3μs (463 nm)	367
O2-Pt	255, 264, 288, 344, 365^{sh}	396,494, 531, 569/493,525,549	0.06	0.45 ns (396 nm)/123.5 μs (493 nm)	384
S2-Pt	261, 269^{sh}, 296, 329^{sh}, 341	397, 494, 531, 578/493,527,549	0.04	0.66 ns (397 nm)/129.8 μs (493 nm)	380
PO2-Pt	248, 293, 341^{sh}, 358	394^{sh}, 409, 436, 507, 542/503, 541, 561	0.03	2.30 ns (409 nm)/293.8μs (503 nm)	396

[a] Measured in CH_2Cl_2 at a concentration of *ca.* 10^{-5} M. sh: Shoulder.
[b] Measured using quinine sulfate in 1.0 M H_2SO_4 as the standard. According to the UV–vis absorption of the compounds, the excitation wavelength was set at 334 nm and 365 nm while the Φ_F of the standard is 56% and 55%.
[c] The numbers in parentheses are the emission wavelengths of the S_1 and T_1 states. The lifetime of the S_1 state was measured at 298 K in degassed CH_2Cl_2 with the excitation at 360 nm and that for the T_1 states was measured at 77 K in the same solvent with the same excitation wavelength.

Table 2
TD-DFT results for the repeating units of the Pt(II) polyynes based on their optimized S_0 geometries.

Compound	Contribution of d_π orbitals to HOMO[a] (Pt)	Contribution of d_π orbitals to LUMO[a] (Pt)	Largest coefficient in the CI expansion of the S_1 state[b]	Percentage contribution of the transition to the S_1 state[b]	Oscillator strength (*f*) of the $S_0 \rightarrow S_1$
C1-Pt	6.58%	0.42%	H→L (0.66026) 372 nm	87.2%	1.6005
O1-Pt	7.00%	0.42%	H→L (0.67379) 363 nm	90.8%	1.5427
S1-Pt	7.20%	0.41%	H→L (0.67030) 363 nm	89.8%	1.6060
PO1-Pt	11.30%	1.66%	H→L (0.66028) 405 nm	87.2%	1.4465
C2-Pt	9.14%	0.16%	H→L (0.65121) 332 nm	84.8%	0.0971
O2-Pt	9.52%	0.00%	H→L (0.63183) 335 nm	79.8%	0.0337
S2-Pt	8.34%	0.00%	H→L (0.59508) 339 nm	70.8%	0.0179
PO2-Pt	10.10%	0.22%	H→L (0.66872) 363 nm	89.4%	0.3923

[a] The data were obtained by exporting DFT results with the software AOMix.
[b] H→ L represents the HOMO to LUMO transition. CI stands for configuration interaction.

2H, Ar), 7.64 (d, 2H, Ar), 7.37 (d, 2H, Ar), 2.20 (br, 12H, PBu_3), 1.68 (br, 12H, PBu_3), 1.48–1.47 (m, 12H, PBu_3), 0.95 (t, 18H, PBu_3); ^{31}P NMR (161.9 MHz, $CDCl_3$): δ (ppm) 3.30; GPC: $M_n = 1.7 \times 10^4$ g mol^{-1}, PDI = 2.2 (against polystyrene standards).

PO2-Pt: (Yield: 85%) ^1H NMR (400 MHz, $CDCl_3$): δ (ppm) 7.66–7.61 (m, 4H, Ar), 7.57–7.46 (m, 4H, Ar), 7.38 (m, 3H, Ar), 2.12 (br, 12H, PBu_3), 1.63 (br, 12H, PBu_3), 1.49–1.40 (m, 12H, PBu_3), 0.93 (m, 18H, PBu_3); ^{31}P NMR (161.9 MHz, $CDCl_3$): δ (ppm) 33.06, 3.70; GPC: $M_n = 1.9 \times 10^4$ g mol^{-1}, PDI = 1.6 (against polystyrene standards).

3. Results and discussion

3.1. Synthesis and structural characterization

Scheme 1 shows the chemical structures and the synthetic pathways of the Pt(II) polyynes. Schemes S1 and S2 in ESI provide the preparation of the ethynyl aromatic ligands. The designed Pt(II) polyynes can be easily prepared using the Sonogashira cross-coupling procedure between the different ethynyl aromatic ligands and *trans*-[$PtCl_2(PBu_3)_2$] in Et_3N with CuI as catalyst (Scheme 1). The chemical structures of these Pt(II) polyynes have been fully characterized by ^1H and ^{31}P NMR spectra. In the ^1H NMR spectra of these Pt(II) polyynes, the absence of the singlet peak at *ca.* 3.2 ppm assigned to the proton in the alkyne groups indicates the successful coupling between the alkyne groups in the aromatic ligands and *trans*-[$PtCl_2(PBu_3)_2$] units. In the ^{31}P NMR spectra of these Pt(II) polyynes, the strong single resonance peaks in the range of 3.12–3.83 ppm indicates the presence of the *trans*-[$PtCl_2(PBu_3)_2$] units. For **PO1-Pt** and **PO2-Pt**, the resonance peak at *ca.* 33.0 ppm in their ^{31}P NMR spectra can be assign to the POPh units in their organic ligands.

3.2. Photophysical properties

The absorption properties of the Pt(II) polyynes were measured in CH_2Cl_2 at 298 K (Fig. 1) and the corresponding data are summarized in Table 1. Obviously, the maximum absorption wavelengths (λ_{max}) of the Pt(II) polyynes bearing fluorene-type ligands with ethynyl units at 3,6-positon (Series 2) show blue-shift effect compared with those of corresponding Pt(II) polyynes with ethynyl units at 2,7-positon (Series 1) (Table 1). The cut-off absorption wavelengths ($\lambda_{cut\text{-}off}$) of the Pt(II) polyynes in Series 2 also show blue-shift effect compared with the Pt(II) polyynes in Series 1. Moreover, the λ_{max} and $\lambda_{cut\text{-}off}$ of the fluorene-type ligands with ethynyl units at 3,6-position also show blue-shift effect compared with those bearing ethynyl units at 2,7-position (Fig. S1 and Table S1 in ESI). These results indicate that ethynyl units at 2,7-position of the fluorene-type ligands are more conducive to extend the π-conjugation in both the Pt(II) polyynes and the ethynyl aromatic ligands. In addition, the absorption bands of the Pt(II) polyynes in Series 2 are nearly located in the UV region (Fig. 1b and Table 1), indicating their excellent transparency in the visible-light region (*ca*. 400–700 nm). However, the Pt(II) polyynes in Series 1 show inferior transparency in the visible-light region than those in Series 2 due to their obvious absorption after 400 nm. In addition, the major absorption bands of **PO1-Pt** and **PO2-Pt** can show red-shift effect compared with other Pt(II) polyynes in the same series, due to the electron-withdrawing property of the P=O unit.

It has been shown that the transition metal polyynes can show similar transition properties to their repeating units [31]. So, the molecular orbital (MO) patterns of the repeating unit for the corresponding the Pt(II) polyynes have been obtained theoretically by time-dependent density functional theory (TD-DFT) calculations to understand their absorption behavior (Fig. 1). Based on the TD-DFT results in Table 2, the transitions between the key molecular orbitals can show the feature of the first singlet state (S_1) of the repeating units of these Pt(II) polyynes due to their large contributions to the transition of the S_1 state. From the MO distributions of both HOMO and LUMO for the repeating units of these Pt(II) polyynes, it can be clearly seen that their HOMO → LUMO (H → L) transition show obvious ligand-centered $\pi-\pi^*$ character (Fig. 2). Therefore, the UV absorption of these Pt(II) polyynes can be assigned to the metal disturbed $\pi-\pi^*$ transitions from the ethynyl aromatic ligands (Fig. 1). In addition, due to their higher extent of electron delocalization in their HOMO orbitals, the repeating units of the Pt(II) polyynes in Series 1 show longer conjugation than those of the Pt(II) polyynes in Series 2. This adequately explains the red-shift effect in absorption maxima of the Pt(II) polyynes in Series 1 compared with corresponding Pt(II) polyynes in Series 2. Owing to the strong electron-accepting ability associated with the five-membered ring of phosphole oxide indicated by its substantial contribution to the LUMO (Fig. 2), it should promote H → L electron transition in **PO1-Pt** and **PO2-Pt** and lower absorption energy associated with the electron transition process. Hence, the red-shift effect has been observed in the absorption spectra of **PO1-Pt** and **PO2-Pt** compared other with other Pt(II) polyynes of the same series (Fig. 1).

In CH_2Cl_2 solution at 298 K, all the Pt(II) polyynes exhibit two emission bands in the PL spectra (Fig. 3 and Table 1). Because of their short lifetimes in the order of nanosecond (ns) (Table 1), the high-energy emission bands should be induced by the decay of the singlet states (S_1) associated with the metal disturbed organic ligand $\pi-\pi^*$ transitions. Conversely, the long-wavelength emission bands should come from the decay of the triplet states (T_1) due to their much longer lifetimes in the order of microsecond (μs) and large Stokes shift (>150 nm). The long-wavelength emission signals of all the Pt(II) polyynes have been substantially enhanced in

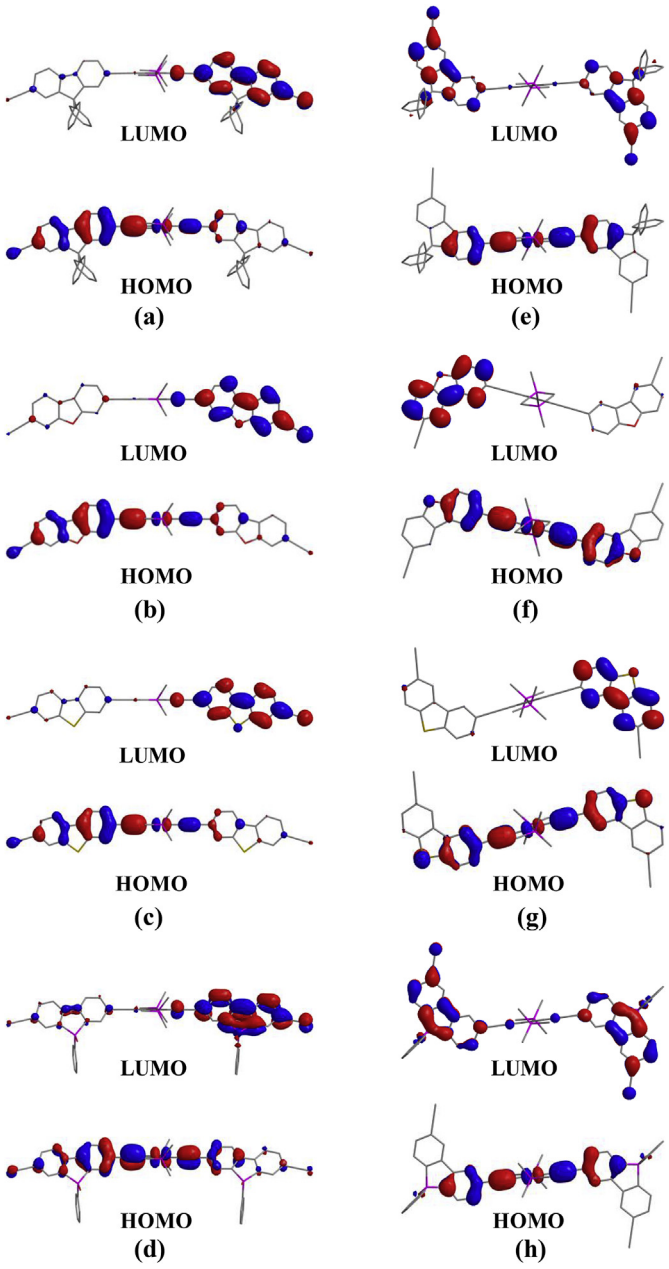

Fig. 2. Molecular orbital (MO) patterns for the repeating units of the Pt(II) polyynes based on their optimized S_0 geometries. (a) repeating unit for **C1-Pt**, (b) repeating unit for **O1-Pt**, (c) repeating unit for **S1-Pt**, (d) repeating unit for **PO1-Pt**, (e) repeating unit for **C2-Pt**, (f) repeating unit for **O2-Pt,** (g) repeating unit for **S2-Pt**, (h) repeating unit for **PO2-Pt**.

solution at low temperature of 77 K, indicating their T_1 characters as well. Obviously, the Pt(II) polyynes in Series 2 show stronger triplet emission and lower Φ_F compared with their corresponding Pt(II) polyynes in Series 1, which means the Pt(II) polyynes in Series 2 have higher triplet quantum yield. Due to the longer conjugation length of the fluorene-type ligands of ethynyl units at 2,7-position, the $S_0 \rightarrow S_1$ transition of the repeating units of the Pt(II) polyynes in Series 1 is spatially further away from the Pt(II) center than those of the repeating units of the Pt(II) polyynes in Series 2, reducing their SOC effect and hence triplet quantum yield [10]. Meanwhile, compared with those of the repeating units of the Pt(II) polyynes in Series 1, d_π orbitals of the Pt(II) centers can give more contribution to the HOMOs of the repeating units of the Pt(II) polyynes in Series

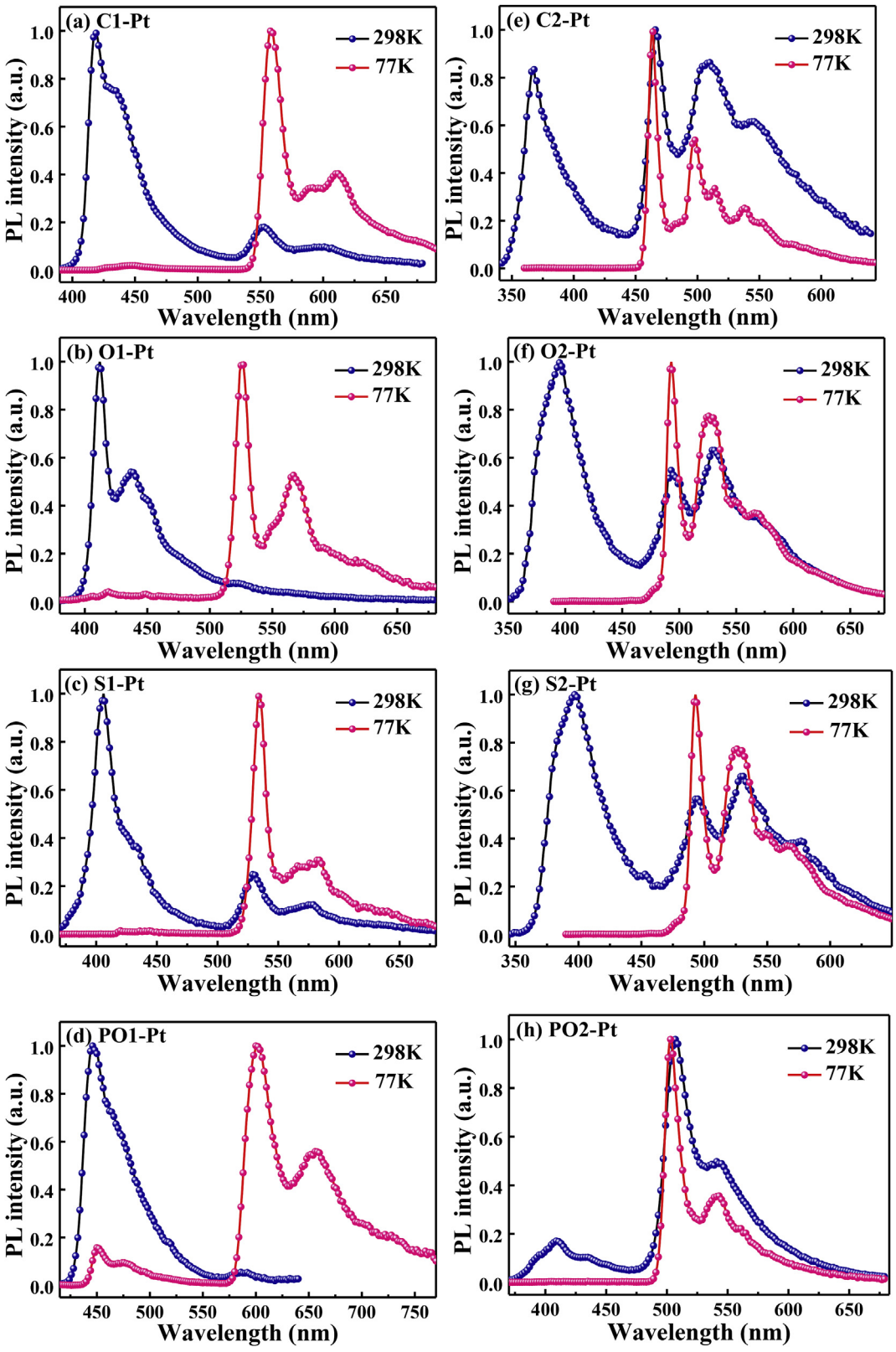

Fig. 3. Photoluminescent (PL) spectra for the Pt(II) polyynes in CH_2Cl_2 solution at both 298 K and 77 K.

2 (Table 2). It means that higher mixing extent between MOs from the Pt(II) centers and organic ligands to guarantee stronger SOC effect in the Pt(II) polyynes of Series 2. As a result, the Pt(II) polyynes in Series 2 can furnish higher triplet quantum yield indicated by the much stronger triplet emission even at 298 K (Fig. 3).

The natural transition orbital (NTO) results for the repeating units of these Pt(II) polyynes have been obtained based on the optimized T_1 geometries for the $S_0 \rightarrow T_1$ excitation [32], which can indicate the features of their triplet emission. From the NTO patterns for the repeating units of the Pt(II) polyynes in Series 1 (Fig. 4), both their hole (H) and particle (P) are mainly located on the ethynyl aromatic ligands on one side of the Pt(II) centers (Table 3). Hence, the H→P transition should indicate the ligand-centered $^3\pi$–π^* character for the triplet emission in the Pt(II) polyynes of Series 1. For the repeating units of the Pt(II) polyynes in Series 2, two pairs of main H→P transitions account for their $S_0 \rightarrow T_1$ excitation (Fig. 4). Clearly, both of the two pairs of H→P transitions are mainly located on the two ethynyl aromatic ligands. From the NTO results in Table 3, the Pt(II) centers in polyynes of Series 1 and 2 make very slight contributions to their H→P transitions responsible for the T_1 emission. Hence, the T_1 emission of these Pt(II) polyynes should mainly show ligand-centered $^3\pi$-π^* feature, which has been indicated by the structured line-shape of their PL spectra at 77 K (Fig. 3). The results show good consistency between the experimental results and the theoretical results, which reflects the validity of the theoretical calculation.

3.3. Optical power limiting behaviors

From the UV–vis spectra of the Pt(II) polyynes (Fig. 1), it can be clearly seen that they exhibit high transparency at 532 nm, indicating their low ground-state absorption at 532 nm. Hence, their absorption behaviors are suitable to characterize their OPL properties against 532 nm laser beam. The OPL performances of these Pt(II) polyynes have been characterized in CH_2Cl_2 with a high linear transmittance of T_o ~94% through *Z*-scan method with an open-aperture mode. From the *Z*-scan curves (Fig. 5), it can be seen

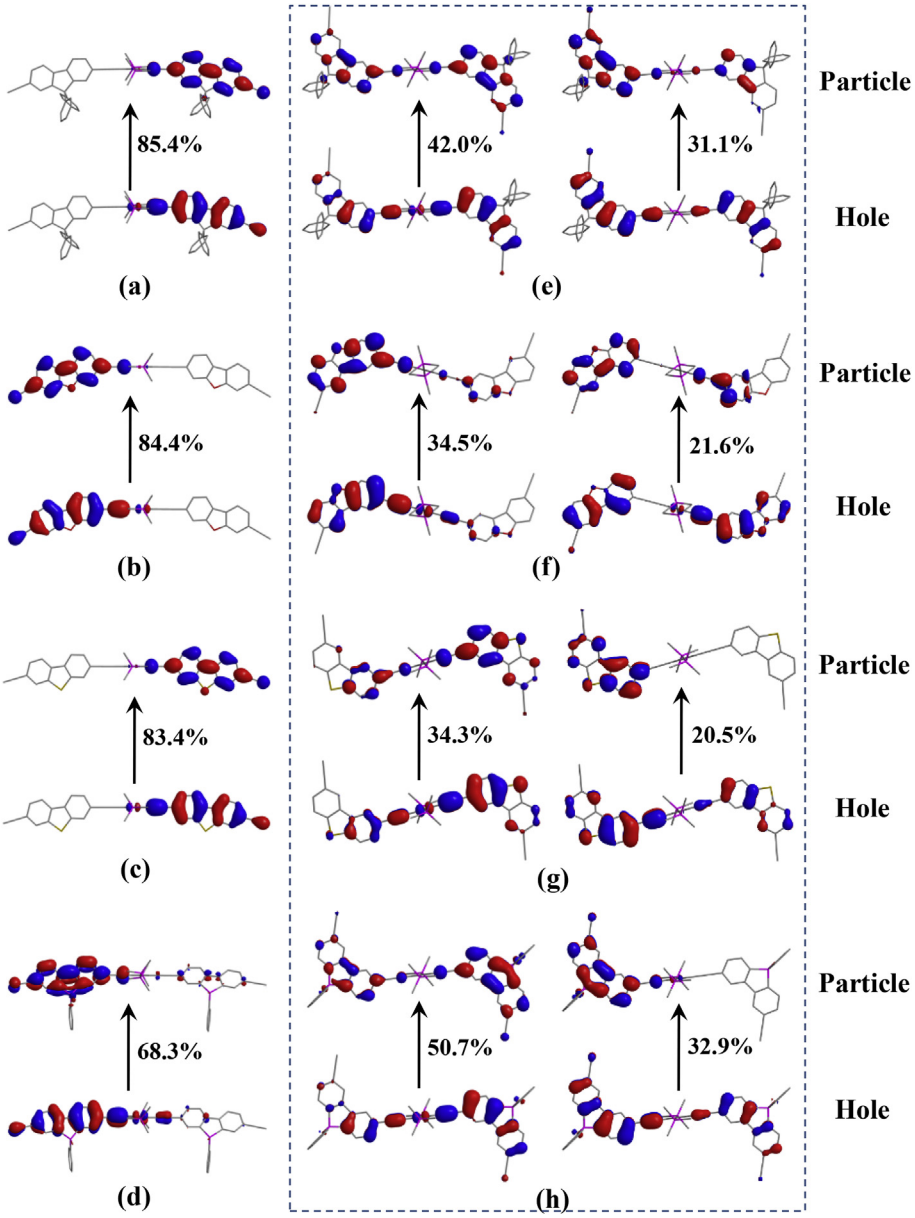

Fig. 4. Natural transition orbital (NTO) patterns for $S_0 \rightarrow T_1$ excitation of the repeating units from the Pt(II) polyynes based on their optimized T_1 geometries. (a) repeating unit for **C1-Pt**, (b) repeating unit for **O1-Pt**, (c) repeating unit for **S1-Pt**, (d) repeating unit for **PO1-Pt**, (e) repeating unit for **C2-Pt**, (f) repeating unit for **O2-Pt,** (g) repeating unit for **S2-Pt,** (h) repeating unit for **PO2-Pt**.

Table 3
NTO results for the repeating units from the Pt(II) polyynes based on the T_1 geometries.

Compound	NTO[a]	Contribution percentages of metal dπ orbitals and π orbitals of ligands to NTOs[b] (%)			Compound	NTO[a]	Contribution percentages of metal dπ orbitals and π orbitals of ligands to NTOs[b] (%)		
		Pt	L1	L2			Pt	L1	L2
C1-Pt	H	2.06	95.90	1.08	**C2-Pt**	H1	2.88	53.43	37.94
						P1	0.37	59.21	38.99
	P	0.65	97.97	0.95		H2	0.10	59.55	37.97
						P2	0.58	60.00	38.99
O1-Pt	H	2.36	95.18	1.40	**O2-Pt**	H1	3.00	85.42	10.61
						P1	0.83	87.48	10.88
	P	0.67	97.59	1.29		H2	1.10	49.07	49.07
						P2	0.33	48.80	48.80
S1-Pt	H	2.35	95.24	1.36	**S2-Pt**	H1	3.82	72.53	22.62
						P1	0.91	74.59	23.43
	P	0.67	97.63	1.24		H2	0.48	68.21	29.69
						P2	1.01	69.25	29.18
PO1-Pt	H	3.96	85.66	9.67	**PO2-Pt**	H1	3.67	65.57	29.98
						P1	0.32	67.99	31.04
	P	1.19	87.81	10.39		H2	0.23	66.75	31.37
						P2	0.78	67.84	31.04

[a] H and P represent NTO hole and particle orbital, respectively.
[b] Pt represent the Pt(II) centers, while L1 and L2 indicate the ethynyl aromatic ligands.

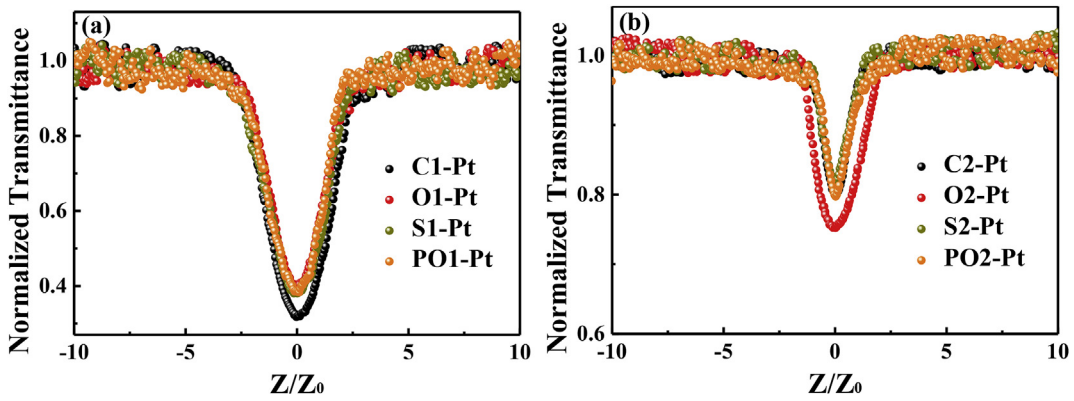

Fig. 5. Open-aperture *Z*-scan results for the Pt(II) polyynes (T_o ~94%). (a) Series 1: **C1-Pt**, **O1-Pt**, **S1-Pt** and **PO1-Pt** (b) Series 2: **C2-Pt**, **O2-Pt**, **S2-Pt** and **PO2-Pt**.

that the incident irradiance upon the Pt(II) polyynes solution sample was changed with their *Z*-position (against focal point $Z = 0$). When the sample stays far from the focal point with the weak incident laser irradiance, the *T* of the Pt(II) polyyne solution can remains constant, indicting linear optical property (*i.e.* obeying Beer's law). However, when the sample is gradually moved towards the focus with the incident laser irradiance increase, the *T* of the sample decreases to show OPL effect (Fig. 5).

Based on the aforementioned photophysical properties, the OPL performance of these Pt(II) polyynes can be explained by the reverse saturable absorption (RSA) mechanism of the T_1 states (Fig. S2 in ESI) [10]. The molecular in the ground state (S_0) can be excited to the first singlet states (S_1) by initially absorbing laser energy of laser irradiance. The S_1 state can go to the first triplet state (T_1) through intersystem crossing (ISC) process due to the strong SOC effect induced by the Pt(II) centers. The T_1 states with long lifetime in micro-second range can easily accumulate a certain population through fast ISC process and then absorb more laser energy to reach the higher triplet states (T_n) in a laser pulse duration of nano-second order. Due to the short lifetime of the S_1 state, the contribution of the OPL effect from optical absorption accompanied with the $S_1 \rightarrow S_n$ transition are generally neglected. Hence, the $T_1 \rightarrow T_n$ transition leads to the OPL effect of these Pt(II) polyynes (Fig. S2 in ESI).

The OPL performances of these Pt(II) polyynes based on the RSA mechanism can be compared by using the figure of merit factor $\sigma_{ex}/\sigma_o = \ln T_{sat}/\ln T_o$ [33], where σ_o and σ_{ex} represent the ground-state absorption cross-section and the effective excited-state absorption cross-section, respectively. T_o and T_{sat} are the linear transmittance and the transmittance at the saturation fluence, respectively. From the *Z*-scan results, the σ_{ex}/σ_o values of **C1-Pt**, **O1-Pt**, **S1-Pt** and **PO1-Pt** are 16.0, 14.5, 12.9 and 14.7, respectively. In addition, the σ_{ex}/σ_o values of **C2-Pt**, **O2-Pt**, **S2-Pt** and **PO2-Pt** are 4.9, 6.0, 4.8 and 4.9, respectively. Owing to their longer conjugation indicated by their UV absorption spectra, the Pt(II) polyynes in Series 1 show stronger OPL responses than those in Series 2. However, based on the RSA mechanism and their stronger triplet emission at 298 K, the Pt(II) polyynes in Series 2 should show better OPL ability for 532 nm ns laser than those in Series 1. This result can be ascribed to their too low ground-state absorption at 532 nm to induce strong enough OPL response. Critically, the excellent transparency in visible light region still render the Pt(II) polyynes in Series 2 good candidates as OPL materials. Hence, the position of the ethynyl units at 2,7- and 3,6-position of fluorene-type ligands have a great influence on the OPL behavior of the Pt(II) polyynes.

4. Conclusions

Two series of Pt(II) polyynes bearing fluorene-type ligands with two ethynyl units at different position were successfully synthesized. Compared with the Pt(II) polyynes (Series 1) bearing ligands with ethynyl units at 2,7-position, the Pt(II) polyynes (Series 2) bearing ligands with ethynyl units at 3,6-position show blue-shift effect in their absorption maxima and much stronger triplet emission. Moreover, the OPL performances of the Pt(II) polyynes can be tuned by the substitution position of the ethynyl units as well. The Pt(II) polyynes in Series 1 can show enhanced OPL response, while those in Series 2 exhibit much better transparency in visible light region. The above results can provide very helpful information to controlling the photophysical properties and OPL ability of the Pt(II) polyynes by designing organic acetylide ligands.

Acknowledgement

This research was financially supported by the National Natural Science Foundation of China (no. 21572176, 21602170), the Fundamental Research Funds for the Central Universities (cxtd2015003, xjj2016061), the Key Creative Scientific Research Team in Yulin City, Shaanxi Province, the China Postdoctoral Science Foundation (2015M580831) and the Program for New Century Excellent Talents in University, the Ministry of Education of China (NECT-09-0651). The financial supporting from State Key Laboratory for Mechanical Behavior of Materials is also acknowledged. The characterizations of materials are supported by Instrument Analysis Center of Xi'an Jiaotong University.

Appendix A. Supplementary data

Supplementary data to this article can be found online at https://doi.org/10.1016/j.jorganchem.2019.05.022.

References

[1] G.R. Whittell, M.D. Hager, U.S. Schubert, I. Manners, Nat. Mater. 10 (2011) 176–188.
[2] Z. Huang, B. Liu, J. Zhao, Y. He, X. Yan, X. Xu, G. Zhou, X. Yang, Z. Wu, RSC Adv. 5 (2015) 36507–36519.
[3] L. Xu, C.-L. Ho, L. Liu, W.-Y. Wong, Coord. Chem. Rev. 373 (2018) 233–257.
[4] W.-Y. Wong, C.L. Ho, Acc. Chem. Res. 43 (2010) 1246–1256.
[5] H. Zhang, X. Yan, J. Zhao, X. Yang, Z. Huang, G. Zhou, Y. Wu, RSC Adv. 5 (2015) 88758–88766.
[6] Q. Dong, Z. Meng, C.-L. Ho, H. Guo, W. Yang, I. Manners, L. Xu, W.-Y. Wong, Chem. Soc. Rev. 47 (2018) 4934–4953.
[7] B. Jiang, L.J. Chen, G.Q. Yin, Y.X. Wang, W. Zheng, L. Xu, H.-B. Yang, Chem. Commun. 53 (2016) 172–175.
[8] G. Zhou, W.-Y. Wong, Chem. Soc. Rev. 40 (2011) 2541–2566.
[9] C.L. Ho, Z.Q. Yu, W.-Y. Wong, Chem. Soc. Rev. 45 (2016) 5264–5295.
[10] G. Zhou, W.-Y. Wong, S.-Y. Poon, C. Ye, Z. Lin, Adv. Funct. Mater. 19 (2009) 531–544.
[11] J.S. Dhindsa, R.R. Maar, S.M. Barbon, M. Olivia Aviles, Z.K. Powell, F. Lagugne-Labarthet, J.B. Gilroy, Chem. Commun. 54 (2018) 6899–6902.
[12] C.-L. Ho, W.-Y. Wong, Coord. Chem. Rev. 257 (2013) 1614–1649.
[13] C.-L. Ho, W.-Y. Wong, Coord. Chem. Rev. 255 (2011) 2469–2502.
[14] T. Kindahl, P.G. Ellingsen, C. Lopes, C. Brannlund, M. Lindgren, B. Eliasson, J. Phys. Chem. A 116 (2012) 11519–11530.
[15] T. Kindahl, J. Öhgren, C. Lopes, B. Eliasson, Tetrahedron Lett. 54 (2013) 2403–2408.
[16] S. Goswami, G. Wicks, A. Rebane, K.S. Schanze, Dalton Trans. 43 (2014) 17721–17728.
[17] M. An, X. Yan, Z. Tian, J. Zhao, B. Liu, F. Dang, X. Yang, Y. Wu, G. Zhou, Y. Ren, L. Gao, J. Mater. Chem. C 4 (2016) 5626–5633.
[18] D. Dini, M.J. Calvete, M. Hanack, Chem. Rev. 116 (2016) 13043–13233.
[19] Y. Du, N. Dong, M. Zhang, B. Jiang, N. Sun, Y. Luo, S. Zhang, G. Wang, J. Wang, J. Mater. Chem. C 6 (2018) 7317–7325.
[20] W.-Y. Wong, L. Liu, J. Shi, Angew. Chem. Int. Ed. 42 (2003) 4064–4068.
[21] W.-Y. Wong, S.Y. Poon, A.W. Lee, J.X. Shi, K.W. Cheah, Chem. Commun. 0 (2004) 2420–2421.
[22] G. Zhou, W.-Y. Wong, D. Cui, C. Ye, Chem. Mater. 17 (2005) 5209–5217.
[23] G. Zhou, W.-Y. Wong, Z. Lin, C. Ye, Angew. Chem. Int. Ed. 45 (2006) 6189–6193.
[24] W.-Y. Wong, J. Inorg. Organomet. P. 15 (2005) 197–219.
[25] C.-L. Ho, S.-Y. Poon, P.-K. Lo, M.-S. Wong, W.-Y. Wong, J. Inorg. Organomet. Polym. 23 (2013) 206–215.
[26] W.R. Dawson, M.W. Windsor, J. Phys. Chem. 72 (1968) 3251–3260.
[27] P.J. Hay, J. Chem. Phys 82 (1985) 299–310.
[28] P.J. Hay, W.R. Wadt, J. Chem. Phys. 82 (1985) 284–298.
[29] M.J. Frisch, G.W. Trucks, H.B. Schlegel, G.E. Scuseria, M.A. Robb, J.R. Cheeseman, J.A. Montgomery, T. Vreven Jr., K.N. Kudin, J.C. Burant, J.M. Millam, S.S. Iyengar, J. Tomasi, V. Barone, B. Mennucci, M. Cossi, G. Scalmani, N. Rega, G.A. Petersson, H. Nakatsuji, M. Hada, M. Ehara, K. Toyota, R. Fukuda, J. Hasegawa, M. Ishida, T. Nakajima, Y. Honda, O. Kitao, H. Nakai, M. Klene, X. Li, J.E. Knox, H.P. Hratchian, J.B. Cross, V. Bakken, C. Adamo, J. Jaramillo, R. Gomperts, R.E. Stratmann, O. Yazyev, A.J. Austin, R. Cammi, C. Pomelli, J.W. Ochterski, P.Y. Ayala, K. Morokuma, G.A. Voth, P. Salvador, J.J. Dannenberg, V.G. Zakrzewski, S. Dapprich, A.D. Daniels, M.C. Strain, O. Farkas, D.K. Malick, A.D. Rabuck, K. Raghavachari, J.B. Foresman, J.V. Ortiz, Q. Cui, A.G. Baboul, S. Clifford, J. Cioslowski, B.B. Stefanov, G. Liu, A. Liashenko, P. Piskorz, I. Komaromi, R.L. Martin, D.J. Fox, T. Keith, M.A. Al-Laham, C.Y. Peng, A. Nanayakkara, M. Challacombe, P.M.W. Gill, B. Johson, W. Chen, M.W. Wong, C. Gonzalez, J.A. Pople, Gaussian 09, Revision A.2, Gaussian, Inc., Wallingford, CT, 2009.
[30] J. Zhang, Y. Ou, M. Xu, C. Sun, J. Yin, G.-A. Yu, S.H. Liu, Eur. J. Inorg. Chem. (2014) 2941–2951, 2014.
[31] G. Zhou, Y. He, B. Yao, J. Dang, W.-Y. Wong, Z. Xie, X. Zhao, L. Wang, Chem. Asian J. 5 (2010) 2405–2414.
[32] Z. Tian, X. Yang, B. Liu, J. Zhao, D. Zhong, Y. Wu, G. Zhou, W.-Y. Wong, J. Mater. Chem. C 6 (2018) 6023–6032.
[33] J.W. Perry, K. Mansour, S.R. Mardar, K.J. Perry, D. Alvarez Jr., I. Choong, Opt. Lett. 19 (1994) 625–627.